Available online at BCREC website: https://bcrec.id

Bulletin of Chemical Reaction Engineering & Catalysis, 17 (2) 2022, 363-374

Research Article

The Effect of Zinc Oxide Supported on Gelatin Mesoporous Silica (GSBA-15) on Structural Character and Their Methylene Blue Photodegradation Performance

Maria Ulfa*, Ida Setiarini

Chemistry Education Study Program, Faculty of Teacher Training and Education, Sebelas Maret University, Jl. Ir. Sutami 36A, Surakarta 57126, Indonesia.

Received: 21st February 2022; Revised: 21st April 2022; Accepted: 23rd April 2022
Available online: 6th May 2022; Published regularly: June 2022

Abstract

Gelatin mesoporous silica SBA-15 (GSBA-15) with rod-like morphology has been successfully synthesized by hydrothermal method using P-123:gelatin, then aged at 90 °C for 24 h and calcined at 550 °C for 5 h. GSBA-15 was impregnated with ZnO amounts of 1; 5; and 10 wt% to obtain Zn/GSBA-15. Samples were characterized by X-ray Diffraction (XRD), Fourier Transform Infra Red (FTIR), Scanning Electron Microscopy (SEM), and Brunauer-Emmett-Teller (BET). The efficiency of methylene blue photodegradation was determined by a UV-Vis spectrophotometer. The FTIR result is functional groups of ZnO/GSBA-15, those were Si−O−Si, −OH, Zn−OH, and Zn−O. The morphology of ZnO/GSBA-15 was rod-like, and it consisted of silica, oxygen, and Zn. The surface area and pore volume of GSBA-15 declined (surface area from 520.8 to 351.9 m^2/g and pore volume from 0.707 to 0.564 cm^3/g) after ZnO impregnation due to pore blocking. At the same time, increasing pore diameter (from 2.82 nm to 3.19 nm) and crystallite size (from 5.1 nm to 12.6 nm) were observed due to the overlapping of ZnO-Silica particles. The increasing incorporation of ZnO on the silica GSBA-15 framework increases the photodegradation performance from 88.76% to 94.90% due to the high surface area, functional group rich, and dispersion of ZnO active sites.

Keywords: Photocatalytic; Degradation; ZnO/GSBA-15; photocatalyst mass; methylene blue

How to Cite: M. Ulfa, I. Setiarini (2022). The Effect of Zinc Oxide Supported on Gelatin Mesoporous Silica (GSBA-15) on Structural Character and Their Methylene Blue Photodegradation Performance. *Bulletin of Chemical Reaction Engineering & Catalysis*, 17(2), 363-374 (doi: 10.9767/bcrec.17.2.13712.363-374)

Permalink/DOI: https://doi.org/10.9767/bcrec.17.2.13712.363-374

1. Introduction

One of the textile industry wastes is dye waste, usually containing organic compounds that are difficult to degrade biologically, such as methylene blue [1,2]. The methylene blue is a toxic aromatic hydrocarbon compound ($C_{16}H_{18}ClN_3S$), with the permissible concentration threshold in waters being 5–10 mg/L [3,4] which harms environmental ecosystems [5]. To minimize pollution, several technologies have been employed, such as using conventional physical methods, namely coagulation and flocculation [6], conventional biological methods [7], and advanced methods, such as Fenton [8] ozonation process [9], photocatalytic [10] and adsorption [11]. Among these methods, photocatalytic is considered the most efficient [10].

Zinc oxide (ZnO) is one of the photocatalysts that can be used in photodegradation because it is inert, abundant in nature, non-toxic, inexpen-

* Corresponding Author.
Email: ulfa.maria2015@gmail.com ;
mariaulfa@staff.uns.ac.id (M. Ulfa)

sive to manufacture, environmentally friendly, and can be made under standard reaction conditions with a band gap of 3.17 eV [12]. Previous research explained that ZnO catalysts have degradation performance for methylene blue [13–15]. However, metal oxide as the catalytic center has undergone agglomeration, reducing the catalytic performance [16]. To overcome this matter, the current research focus involves host or supporting materials for metal catalysts such as carbon, silica, and polymers [17–19].

One of the supporting materials widely employed as a ZnO host is mesoporous silica. Its pore size can be adjusted from 2 to 50 nm by template engineering and optimization of reaction conditions [3,4,16]. The other uniqueness of mesoporous silica is that it is inert and has a highly ordered structure, a large pore size, a large specific surface area, thick frame walls, high thermal stability. Moreover, its size can be controlled easily [20]. The use of mesoporous silica as a host of ZnO in the degradation process of methylene blue dyes has been widely studied, such as ZnO/MCM-41 and ZnO/mesoporous silica, which have higher degradation activity than ZnO [3,4]. However, the synthesis of mesoporous silica requires synthetic soft templates, such as CTAB, P123, or F127 [21–23], which have high prices with low levels of sustainability, and their production is complicated and involves many chemicals, some of which require advanced handling at high costs. Several researchers overcame the problem by replacing the use of synthetic templates with environmentally friendly organic materials such as natural gelatin, starch, and gum arabic [23–25].

The previous research has combined gelatin with a synthetic template to produce carbon foam worm-holes, mesoporous carbon microspheres, and hexagonal flake-like hematite with a high surface area of 90 to 220 m^2/g with pore size up to 5–10 nm [11,26,27]. The use of gelatin which contains amine ($-NH_2$) groups that have a high affinity to interact strongly with hydroxyl (OH) by hydrogen bonds, gives advantages as a pore directing agent to produce the unique material in the previous reports [28–31]. So, in this study, the mesoporous silica was synthesized using gelatin. To minimize the synthetic organic template, ZnO metal oxide was impregnated into resulted mesoporous silica from gelatin template (GSSBA-15), and the photodegradation of methylene blue performance was investigated.

2. Materials and Methods

2.1 Materials

All of the chemicals were analytical grade purchased from Sigma Aldrich Co., LLC (St. Louis, USA), such as P123 (MW 5750 g/mol), Commercial Gelatin (MW 90.000 g/mol), TEOS (MW 208.33 g /mol), $Zn(CH_3COO)$, ethanol (pa) and *methylene blue* (MW 319.85 g/mol), and HCl 37% (MW 36.5 g/mol).

2.2 Synthesis of mesoporous silica GSBA-15

Synthesis of mesoporous silica applied gelatin as a template labeled as GSBA-15. It was prepared by adding 4 g of P123 and 0.04 g of gelatin to 19.5 mL of 37% HCl in 127 mL of distilled water. It was then stirred at 40 °C (500 rpm) for 3 h. The 8.62 g of TEOS was added to the mixture, and the stirring was continued for 24 h. The resulting mixture was carried out for hydrothermal process at 90 °C for 24 h in autoclave with Teflon liner (Figure 1). The resulting sample was filtered, washed, and dried for 24 h at 70 °C and followed by a second drying step at 100 °C for 24 h. Finally, the dry sample was calcined in a furnace at 550 °C for 5 h and then labeled as GSBA-15. For activation, 1.5 g of GSBA-15 was mixed with 50 mL of 0.1 M HCl for 24 h. It was then filtered, washed, and dried for 24 h at 100 °C.

2.3 Impregnation of ZnO/GSBA-15

1% of $Zn(CH_3COO)_2.2H_2O$ (0.033716 g) was dissolved in 42 mL of ethanol solvent while stirred with a magnetic stirrer at 70 °C for 2 h. The solution obtained was cooled to room temperature. It was then mixed with a Zinc Oxide (ZnO) solution with 1 gram of activated GSBA-15 while vigorously stirring. Next, it was dried at 80 °C for 24 h for eliminating solvent. It was then calcined in a furnace at a temperature of

Figure 1. Hydrothermal reaction in stainless steel jacket and inner Teflon liner.

550 °C for 4 h to form 1% ZnO/GSBA-15. The number of ZnO ratios was increased to obtain the ZnO:G-SBA ratios of 5% and 10%.

2.4 Photocatalytic Activity of ZnO/GSBA-15

The photocatalytic activity of ZnO/GSBA-15 was evaluated by measuring the degradation of methylene blue in wastewater solution under UV radiation. The experiment was carried out in a photocatalytic reactor in an Erlenmeyer containing 200 mL of the methylene blue solution with an initial concentration of 5 mg.L^{-1}. The 50 mg of ZnO/GSBA-15 samples from each ZnO mass variation were dispersed into the methylene blue solution by shaking for 30 min in the dark to achieve adsorption-desorption equilibrium. The photocatalytic reactor was set up to degrade methylene blue with the black box, which was used to prevent light from surrounding for dark adsorption reaction. Afterward, the mixture was placed vertically under a 300 W Xenon lamp equipped with an optical transmission filter (λ = 365 nm). A total of 10 mL of the suspension was collected at a fixed reaction time and centrifuged to remove the catalyst. The concentration of methylene blue supernatant was determined by measuring the absorbance of the solution at a wavelength of 665 nm with a UV-Vis spectrophotometer (Shimadzu UV-3600). The percentage of methylene blue photodegradation was calculated using the equation as follows:

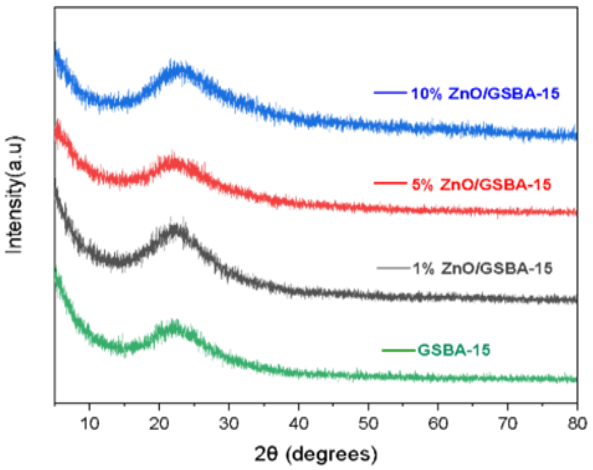

Figure 2. Diffractogram of the GSBA-15, ZnO/GSBA-15 1, 5, and 10 wt% samples.

$$\%Removal = \frac{C_0 - C_t}{C_0} \times 100 \quad (1)$$

where, C_0 and C_t represent methylene blue concentration in the solution before and after the UV irradiation, respectively.

2.5 Characterization of ZnO/GSBA-15

Instruments employed to test samples included X-Ray Diffraction (XRD) brand Pananalytical (version PW3050/60), Fourier Transform Infrared Spectrophotometer (FTIR) brand with a Shimadzu 21 resolution of 0.5 cm^{-1}, Scanning Electron Microscopy-Energy Dispersive X-Ray (SEM-EDX) with a JEOL JSM-700 microscope at a voltage speed of 15.0 kV, a Brunauer-Emmett-Teller (BET) brand Quantacrome Nova 1200e, a Spectrophotometer Ultra Violet Visible (UV-Vis) brand Shimadzu UV-3600 with a wavelength of 665 nm. The crystal size (D) of the samples was calculated by the Debye Scherrer equation (Equation (2)).

$$D = \frac{0.9\lambda}{\beta \cos\theta} \quad (2)$$

D is the crystal size in Å, λ is the wavelength source used in the XRD test (1.54056 Å), and β is the half-peak width in radians. θ is the angular position of the peak formation. The crystallinity of the sample could also be computed by Equation (3).

$$Crystallinity\ (\%) = \frac{crystalline\ peak\ area}{crystalline\ peak\ area + amorphous\ peak\ area} \times 100 \quad (3)$$

3. Results and Discussion

3.1 X-Ray Diffraction (XRD) Characterization

Figure 2 shows the X-ray diffractogram of ZnO/GSBA-15 with ZnO mass ratios of 1, 5, and 10% w/w. The prominent peaks for mesoporous silica (JCPDS-850897) were observed in the amorphous phase at 21.08°, with the miller field (100), which is in accordance with the literature that there is no crystal phase of mesoporous silica GSBA-15. It also exhibits the successfully mesoporous silica synthesized by gelatin addition in the synthetic organic template [20]. When ZnO was increased from 1% to 10%,

Table 1. Crystallite Size of GSBA-15 before and after ZnO incorporation.

Sample	λ (Å)	β (rad)	Peak Position 2θ	%Crystallite	D (nm)
GSBA-15	1.5405	1.398	0.0697	23.3	5.7
ZnO/GSBA-15 1 wt%	1.5405	1.319	0.442	33.3	6.0
ZnO/GSBA-15 5 wt%	1.5405	2.335	0.969	36.7	8.2
ZnO/GSBA-15 10 wt%	1.5405	0.628	0.068	43.4	12.7

there were no significant ZnO peaks (JCPDS 361451) and no differences in mesoporous silica peaks' position. This fact suggests that the low amount of ZnO (according to EDX that Zn is detected close to 1–6%) does not change the stability of mesoporous silica GSBA-15. This opinion is also based on several previous studies reporting that the peak of ZnO in the supporting material was detected by XRD when the mass ratio of ZnO to the supporting material was more than 30–40% w/w [3,14,15,17,32,33]. Further, XRD does not give information regarding the existence of ZnO due to the low content of ZnO, which may be thoroughly dispersed in the mesoporous silica GSBA-15 matrix. Hence, the amorphous structure of mesoporous silica GSBA-15 has a quenched crystal-line structure of ZnO. However, the detection of ZnO can be done by EDX and FTIR, but the structure of mesoporous silica GSBA-15 has been confirmed from nitrogen adsorption-desorption isotherms.

Table 1 shows the effect of the ZnO addition on the crystallite size of the mesoporous silica of GSBA-15, which exhibits an enlargement with the increasing ZnO amounts. It reveals that ZnO has fully dispersed onto the surface of the mesoporous silica and has a significant effect on the crystallite size because ZnO and the resulting silica particles overlap.

During ZnO precursor infiltration, the overlapping particle has been done to the mesopore structure. The overlapping step has a big opportunity to produce a big crystallite size and a larger space as a new pore (Figure 5). The other factor that influences the enlarging crystallite size after ZnO incorporation is the growth of ZnO, which is affected by precipitation rate, Zn-supporting material, and the calcination temperature [40]. The growth of ZnO in GSBA-15 is detected by the change of the crystallite size by XRD before and after impregnation data. In conclusion, the growth of ZnO particles in GBA-15 is governed by increasing the amount of Zn precursor, which has a significant impact on the ZnO distribution, crystallite size, and new space in the composite

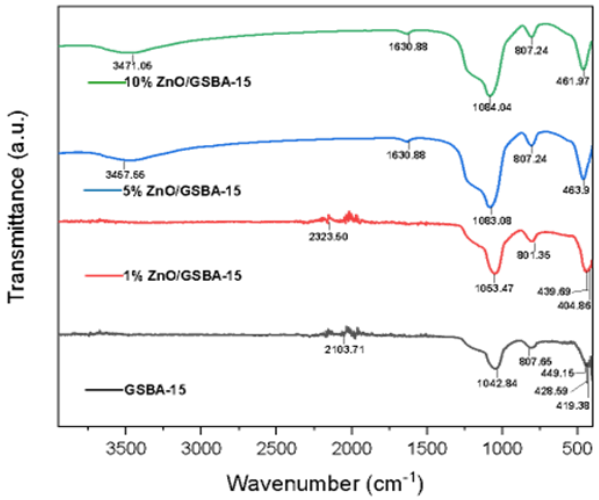

Figure 3. IR spectra of GSBA-15, ZnO/GSBA-15 1, 5, and 10% at wave numbers 450-4000 cm^{-1}.

3.2 Fourier Transform Infrared Spectrophotometer (FTIR) Characterization

Figure 3 displays the FTIR spectra of GSBA-15, which exhibited some significant differences between silica samples before and after ZnO impregnation. The intensity of the peaks at 3381.52–3453.69 cm^{-1} significantly increases for the sample at higher ZnO concentration, suggesting ZnO's influence in increasing hydroxyl region (−OH) of mesoporous silica that is associated with stretching vibrations of the Si−OH group. In the ZnO/GSBA-15 1% and GSBA-15 samples, the absorption bands are observed at 2108.71 cm^{-1} wavenumber, which indicates a stretch of CO_2 due to the partial decomposition of gelatin. The peak at 1630 cm^{-1} corresponds to the bending modes of adsorbed water [16]. The high intensity of mesoporous ribbon character at 1042.84 cm^{-1} is for symmetric modes stretching of lattice vibrations

Table 2. FTIR analysis data from samples GSBA-15, ZnO/GSBA-15 1, 5, and 10 wt%.

Spectra	Wave Number	Type Vibration	Reference
GSBA-15	2108.71	Stretching CO_2	[16]
	1042.84	Stretching Si−O−Si	[16]
	807.65	Stretching Si−O−Si	[36]
	449.15	Si−O	[36]
1% ZnO/GSBA-15	2323.50	Stretching CO_2	[16]
	1053.47	Stretching Si−O−Si	[16]
	801.35	Stretching Si−O−Si	[16]
	439.69	Vibration Zn−O	[35]
	404.86	Vibration Zn−O	[17]

Si–O–Si, and symmetric modes stretching of lattice vibrations at 801 cm^{-1} is O–Si–O [16,33,34]. The absorption peak is also investigated at 420–430 cm^{-1}, representing the characteristic vibrational mode of Zn–O [17,35], which confirms the success of ZnO incorporation onto silica GSBA-15. The FTIR analysis peak in this work is in line with previous research in Table 2.

2.3 Brunauer-Emmett-Teller (BET) Surface Area Characterization

Analysis of surface area using the BET method determines the surface area, pore volume, and pore diameter of GSBA-15 and ZnO/GSBA-15. Based on the BET analysis, the adsorption-desorption curves of GSBA-15, ZnO/GSBA-15 5 and 10 wt% are exposed in Figure 4.

Based on Figure 4, all samples in the adsorption-desorption match with the type IV isotherm of mesoporous materials with hysteresis loop type of H-1, which is related to porous materials with a narrow pore size distribution [16]. Thus, it is apparent that there is an inflection position located at a relative pressure (*P*/*Po*) in the range of 0.4–0.9, which indicates that ZnO loading in GSBA-15 causes a change in the shape of the hysteresis loop. Still, there is no significant difference in the isotherm form between GSBA -15 and ZnO/GSBA-15.

Table 3 presents experimental data based on the analysis of the surface area, pore volume, and pore diameter. Positive correlation results are found in Table 3 where a higher surface area would result in lower pore diameter. It can be seen in the declining surface area from 500.8 to 351.9 m^2/g and pore volume from 0.71 to 0.56 cm^3/g, suggesting that ZnO is confined inside the pores of mesoporous silica GSBA-15. However, the decreasing surface area after impregnation significantly influences the increasing pore size from 2.82 nm to 3.19 nm, which is close to 11.5%. Typically, after impregnation, the pore diameter of silica would be smaller than before due to the pore blocking of ZnO to the silica. However, the increasing pore size after ZnO impregnation is logical due

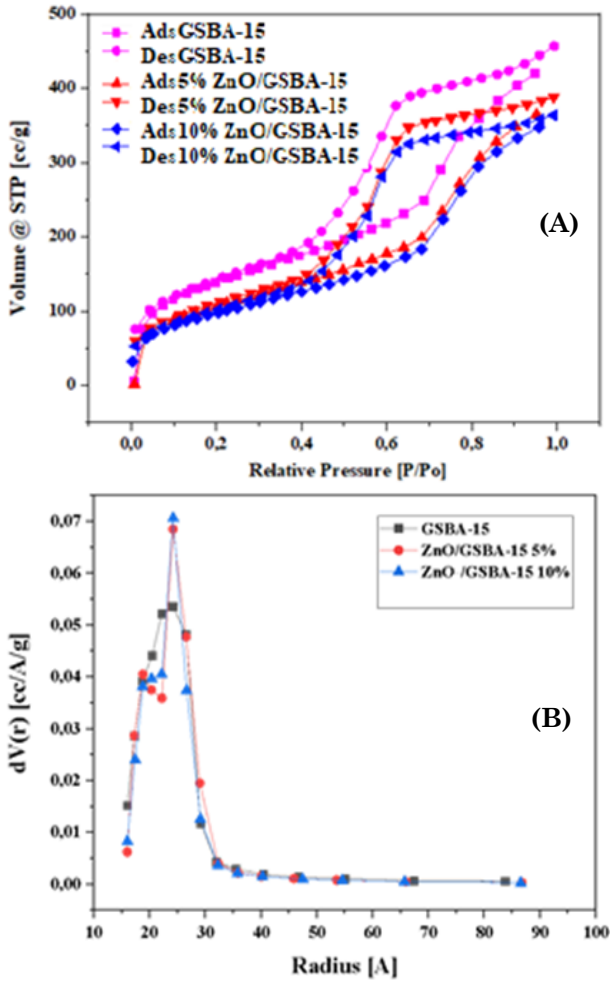

Figure 4. (A) Isotherm adsorption and (B) pore size distribution of ZnO/GSBA-15.

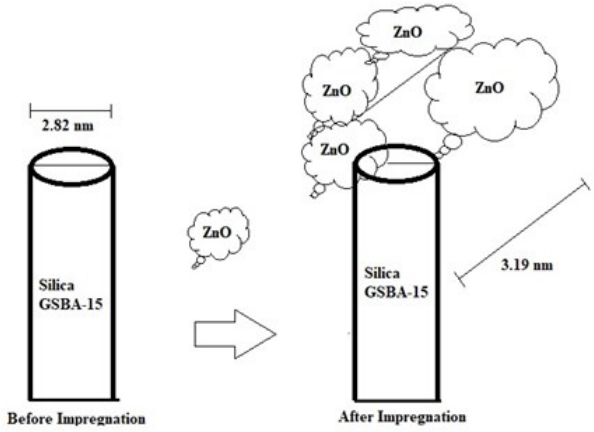

Figure 5. Illustration of pore size silica GSBA-15 after ZnO impregnation.

Table 3. Results of sample porosity analysis using BET characterization.

Sample Type	GSBA-15	5% ZnO/GSBA-15	10% ZnO/GSBA-15
BET Surface Area (m^2/g)	520.8	390.4	351.9
Total Pore Volume (cm^3/g)	0.707	0.602	0.564
Pore Diameter (nm)	2.82	3.07	3.19

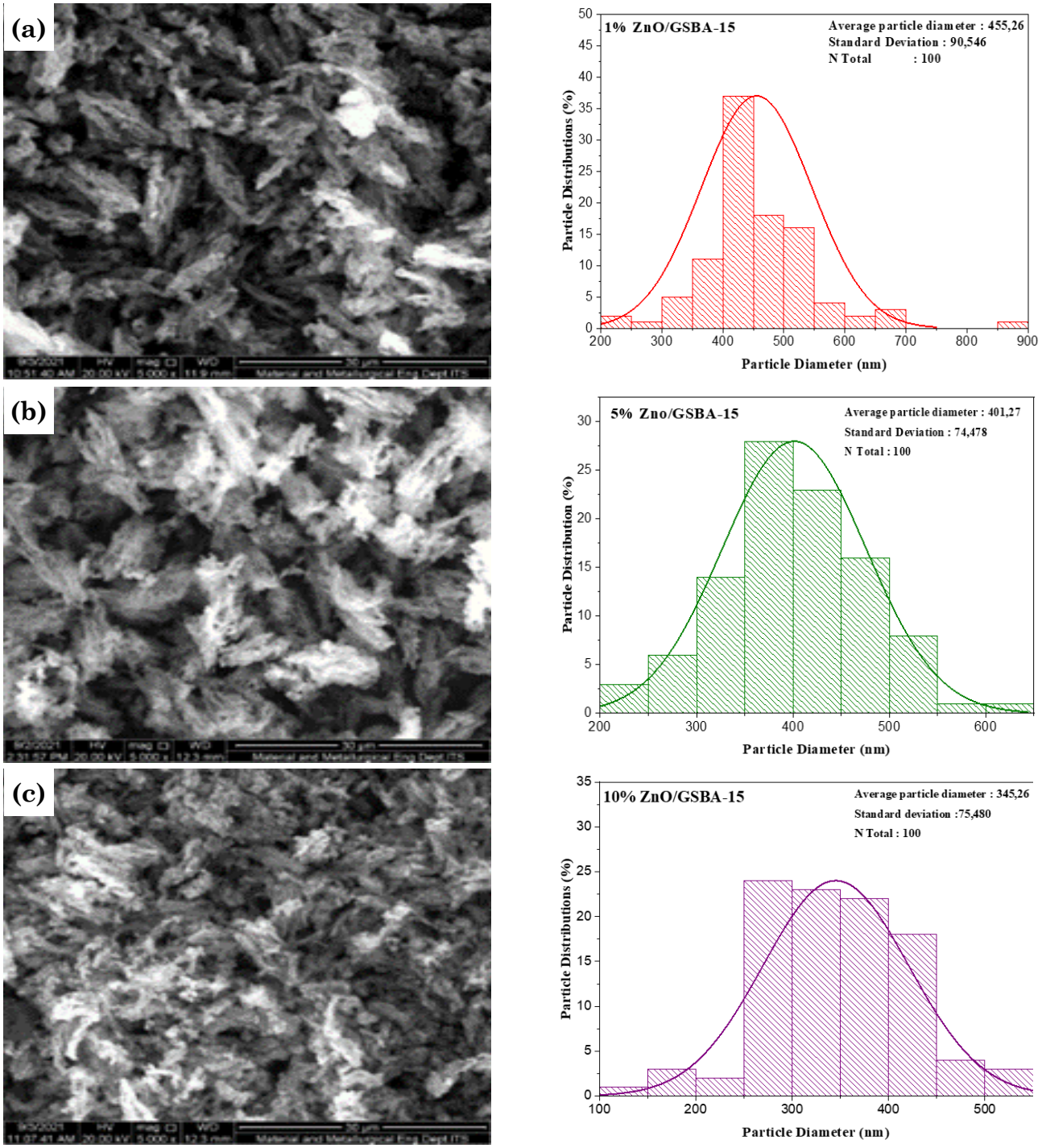

Figure 6. SEM image and particle distribution of (a) ZnO/GSBA-15 1% (b) ZnO/GSBA-15 5% (c) ZnO/GSBA-15 10%.

Table 4. Analysis of elemental composition and average particle diameter of GSBA-15, ZnO/GSBA-15 1, 5, and 10 wt%.

Photocatalyst	Diameter of particle, µm	Elemental Composition Analysis				
		C, %	O, %	Si, %	Al, %	Zn, %
GSBA-15	0.52	9.4	49.03	41.57	–	–
ZnO/GSBA-15 1%	0.46	16.41	49.18	32.79	–	1.62
ZnO/GSBA-15 5%	0.40	6.69	48.24	39.59	–	5.48
ZnO/GSBA-15 10%	0.35	–	45.75	44.42	2.65	6.12

to the overlapping between ZnO-ZnO and ZnO-silica particles to form a larger space as a new pore size (Figure 5).

2.4 Scanning Electron Microscopy-Energy Dispersive X-Ray (SEM-EDX)

SEM characterization was employed to examine the morphology, distribution, and particle shape of GSBA-15, ZnO/GSBA-15 1, 5, and 10 wt% powders. The morphology of all samples is almost the same, giving general information that increasing ZnO incorporated to silica surface amount does not significantly affect the stability of the silica GSBA-15 framework. Figure 5 demonstrates the surface GSBA-15 as the number of white granules pipe as rod-like morphology. According to histogram measurements, the average size of the particles formed is between 345 nm to 525 nm (equal to 0.35-0.53 μm), so it can be concluded that the particles formed are micro-sized. Histogram by SEM reveals that increasing ZnO has a significant effect on decreasing the sharp distribution particle due to the ZnO growth, the overlapping between ZnO and silica particles as the same explanation by XRD. Silica GSBA-15 and ZnO/GSBA-15 are mesoporous samples that are categorized as bulk. The particle size is not identical to the crystallite size in the bulk scale. Crystallite is part of the grain, while the grain is part of the particle, so that the crystallite size < grain (grain) < particle. Therefore, the crystallite sizes of GSBA-15 by XRD are smaller than particle sizes by SEM.

From Table 4, it is apparent that each photocatalyst has the highest percentage of elemental O content, which is more than 45%. In the GSBA-15 photocatalyst, which had been impregnated with ZnO, it was identified the presence of Zn in it so that the Zn impregnation process into GSBA-15 silica was successfully carried out. The percentage of Zn increased significantly with the mass % of Zn contained in GSBA-15, but the content of the Zn10% in ZnO/GSBA-15 photocatalyst was different from the percentage of Zn added, which was only 6.12%. The difference in the percentage of Zn between the experiment and EDX detection is predicted due to the leaching of ZnO during the washing and filtrating step from the GSBA-15 surface. In addition, the incorporation of ZnO onto GSB-15 decreases %C due to the high ZnO insertion during interaction onto silica surface. So, the high ZnO on GSBA-15 can improve the stability of silica during organic decomposition at high temperatures and have a significant influence on reducing carbon.

2.6 Photocatalytic ZnO/GSBA-15

Testing the ZnO's effect onto GSBA-15 as a photocatalyst on the degradation process of methylene blue is to determine which type of photocatalyst is most effective in producing •OH radicals. Figure 6 describes the duration of irradiation in the photodegradation process, which illustrates the effect of the interaction (contact) between photocatalyst and light (hv) in producing •OH radicals and contact between •OH radicals and methylene blue in the degradation process. In dark conditions or when the photocatalyst is at first 30 min, high MB removal values were obtained due to the high surface area of GSBA-15, not only via physical interaction on surface and pore but also chemistry interaction between MB-Silica and MB-Silica-Zn. The second step at min 30 to 90 was the photodegradation reaction in which a total MB removal improved due to the light source as the photon energy to produce •OH radicals. This interaction was strong that the methylene blue was not only adsorbed on the silica surface but also degraded optimally [15,33] due to the excitation of electrons from the conduction band to the valence band by photon, so that any •OH radicals were formed [22]. The total efficiency value of the degradation product using ZnO/GSBA-15 photocatalyst was higher than in the dark condition, concluding the significant effect of ZnO incorporation.

According to Table 5, the value of the degradation efficiency improves with the increase in the ZnO mass. It is in accordance with the pore diameter value in the BET analysis, which also enlarges, so that the absorption of methylene blue is maximized. The mechanism of the degradation reaction of methylene blue in the photocatalyst ZnO and ZnO/GSBA-15 under UV light irradiation can be written as follows:

$$ZnO + hv \rightarrow ZnO\ (e^- + h^+) \quad (1)$$

$$OH- + h^+ \rightarrow OH \quad (2)$$

$$H_2O + h^+ \rightarrow \cdot OH + H^+ \quad (3)$$

Table 5. Efficiency of degradation methylene blue by photocatalysts GSBA-15, ZnO/GSBA-15 1, 5, 10 wt%, and ZnO at 90 min of irradiation time.

Photocatalyst	Degradation Efficiency (%)
GSBA-15	24.80
1% ZnO/GSBA-15	88.76
5% ZnO/GSBA-15	94.90
10% ZnO/GSBA-15	90.40

$$\cdot OH + MB \rightarrow CO_2 + H_2O \quad (4)$$

$$MB + e^- \rightarrow 16CO_2 + 6H_2O + HCl + HNO_3 + H_2SO_4 \quad (5)$$

The activity of ZnO oxide on GSBA-15 as a photocatalyst significantly enhanced MB removal. Before irradiation, the initial adsorption has optimized the interaction between MB and the ZnO-silica surface. The photodegradation process can occur through the direct reaction of hydroxyl radicals with MB adsorbed on the surface of the photocatalyst. The high silica surface area supports the interaction of MB with ZnO/GSBA-15 higher than direct photocatalytic degradation without adsorption. When the ZnO and ZnO/GSBA-15 photocatalysts absorb photons with an energy equal to or greater than the energy width of the ZnO bandgap, then the electrons in ZnO are excited from the valence band to the conduction band. Then, electron-hole pairs are generated. Where, e^- and h^+ are electrons in the conduction band (e^-) and electron vacancies in the valence band (h^+), respectively. These two entities can migrate to the surface of ZnO and ZnO/GSBA-15 and enter into redox reactions with organic pollutants; in this case, it is methylene blue on the surface. Hole electrons will react with H_2O or OH^- to produce a hydroxyl radical ($\cdot OH$). The active radical degrade $N-C_3$ bond then $-CH_3$ is oxidized to HCHO or HCOOH, then active radical break the molecule with C–S and C–N bonds and produce unstable smaller organic as side product. This radical is a powerful oxidizing agent and the primary oxidizer in the photocatalytic oxidation of methylene blue to carbon dioxide, water, and other mineralized products, such as hydrochloric, sulfuric, and nitric acid. Meanwhile, the electrons (e^-) will react with methylene blue to produce reduced products as smaller organic, namely CO_2 and H_2O as primary prod-

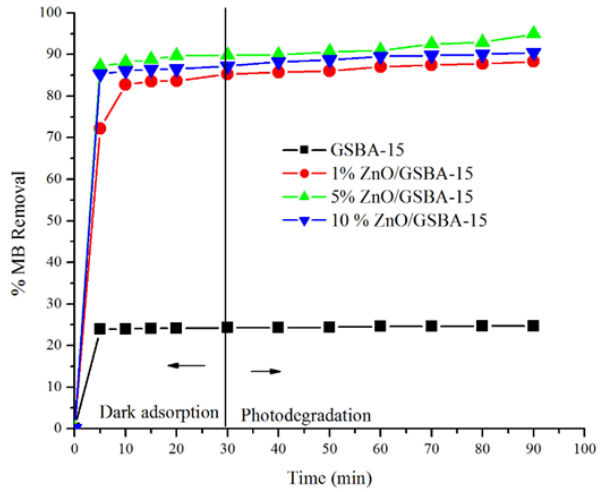

Figure 7. Effect of dark adsorption and irradiation time on the efficiency of degradation methylene blue.

Figure 8. Decolorization performance from 0 min (left) to 90 min (right) on the 10% ZnO/GSBA-15 sample.

Table 6. The effect of dark adsorption and photodegradation on total MB removal.

Time (min)	%MB removal			
	GSBA-15	1% ZnO/GSBA-15	5% ZnO/GSBA-15	10% ZnO/GSBA-15
Dark adsorption				
30	24.3	85.38	89.80	87.19
Photodegradation				
40	24.3	85.72	89.91	88.22
50	24.4	86.06	90.59	88.66
60	24.6	87.08	91.04	89.46
70	24.6	87.42	92.52	89.80
80	24.7	87.76	92.97	90.02
90	24.7	88.32	94.90	90.48
$\Delta t_{90}-t_{30}$	0.40	2.96	5.09	3.28

ucts, and other ion, such as Cl^-, SO_4^{-2} and NO_3, as side product [37,38].

Based on Figures 7 and 8 and Table 6, the degradation of methylene blue (MB) advances with the increase in UV irradiation time. At 0–30 minutes of dark adsorption, there was a reasonably significant increase in degradation, while at 30–90 min, the degradation advanced from 2.96 to 5.09, along with increasing ZnO from 1–5%. The average MB decolorization via dark adsorption and photodegradation using ZnO/SBA-15 achieved 85% and 4%, respectively. This high decolorization during dark adsorption is predicted to come from a high surface area and large pore, which facilitates MB adsorption. However, the % MB removal using GSBA-15 after ZnO impregnation was higher than before due to the inert character of GSBA-15. The inert (neutral character) of GSBA-15 facilitates adsorption of MB species by the pore and interaction between MB and Si−O−Si only, which explains the lower MB removal during dark adsorption than after ZnO incorporation. This result is in line with the previous report [15]. According to the previous research, mesoporous silica had a very small amount of acidic site compared to the silica after ZnO incorporation, in which the acidity increased 8–9 times due to the dispersion of zinc oxide [15]. It clarifies the higher % MB removal of GSBA-15 after incorporating ZnO during dark adsorption, which ZnO on silica surface facilitates the adsorption via strong electrostatic attraction between MB, Si−O−Si, and the active site of ZnO. Thus, it can be concluded that the electrostatic interaction between catalyst surface and MB as organic dyes plays a major role in the dark adsorption step.

From the literature, we found that the band gap of the ZnO bulk is 3.3 eV [32] to 3.3 eV [15]. However, after impregnating onto silica-based material, the band gap of ZnO improved by 3.38 to 4.01 eV from 5–30% ZnO weight [15,32]. This information demonstrates that ZnO/GSBA-15 in this work has the same probability of absorbing light in the UV region. For that reason, we correlated the bandgap information from previous research with the photodegradation performance of ZnO/GSBA15. Figure 6 exhibits that the degradation curve can be divided into two stages. One is a rapid adsorption process from zero min to 30 min. The other is a photocatalytic degradation process from 40 min to 90 min. There is an increasing degradation from 2.9% to 5% due to an increasing ZnO content from 1–5%, as presented in Table 7.

This phenomenon confirms two factors: first, the low content of ZnO in GSBA-15. Previous studies report that 17%TiO_2/SBA-15 achieved 4% photodegradation for 350 min and 58% MB removal via 60 min dark adsorption [39]. Other literature mentioned that ZnO/Silica with amount ZnO 5–20% achieved 85 to 99% of total MB removal from dark adsorption (60–120 min) and photodegradation (120–350 min) which the real ZnO element by EDX is 4.9 to 20.1 %w/w [15,32,33]. However, the photodegradation in our manuscript was higher than in previous studies with higher ZnO content as an active site due to the high surface area of silica GSBA-15 as a supporting catalyst

Another factor is time for dark adsorption and irradiation time. The previous research reported a longer time for both steps and reached

Table 7. The comparative study of %MB removal

Material	Degradation in dark adsorption (%)	Photodegradation after dark adsorption (%)	% w/w Zn by EDX	Total % Removal (Total time dark adsorption + photodegradation)	Ref.
ZnO/SBA-15	50.0 (120 min)	41.0 120 min	30	91.0 (240 min)	[15]
17%TIO_2/SBA-15	58.0 (60 min)	4.0 (150 min)	17	62.0 (90 min)	[39]
15% ZnO/SBA-15	n.d. (10 min)	22.0 (350 min)	19.89	73.0 (360 min)	[33]
1% ZnO/GSBA	85.3 (30 min)	2.9 (60 min)	1.62	88.3 (90 min)	this work
5% ZnO/GSBA	89.8 (30 min)	5.09 (60 min)	5.48	90.4 (90 min)	this work
10% ZnO/GSBA	87.2 (30 min)	3.28 (60 min)	6.12	94.9 (90 min)	this work
5% ZnO/Silica	Not detected	Not detected	4.9	85 (180 min)	[32]
10% ZnO/Silica	Not detected	Not detected	10.2	99 (180 min)	[32]
20% ZnO/Silica	Not detected	Not detected	20.1	85 (180 min)	[32]

total MB removal from 85 to 99%, the same as with ZnO/GSBA-15, which resulted from 88% to 94%. However, the low irradiation time of MB removal by ZnO/GSBA-15 achieved a smaller MB removal than dark adsorption. Hence, the second reason concludes that the lower irradiation time significantly affects the photodegradation performance. However, the higher total MB removal of ZnO/GSBA-15 is not only from the surface area but also from the site active distribution factor. This result is in line with previous research [15,32,33,39].

4. Conclusion

Mesoporous silica (GSBA-15) with rod-like morphology has been successfully synthesized using gelatin and P123 with the template method. Increasing crystallite size and pore diameter of GSBA-15 after ZnO incorporation was due to variation of weight ratios between ZnO and GSBA-15 from 1% to 10%, but the surface area decreased from 520 m^2/g to 345 m^2/g due to the pore blocking and overlapped silica-ZnO particle. The FTIR data of GSBA-15 after impregnation show the formation of Si−O−Si and Zn−OH bonds, and the main element of Si, Zn, and O were observed in EDX. A combination of dark adsorption and photocatalytic degradation of methylene blue using ZnO/GSBA-15 achieved 94%, implying the appropriate catalyst for dye molecule degradation.

Acknowledgments

The authors acknowledge the financial support of the Ministry of Research, Technology and Higher Education Indonesia in Excellence Fundamental Research for University scheme under contract number 221.1/UN27.22/HK 07.00/2021 for Maria Ulfa from Sebelas Maret University

References

[1] Díaz-Uribe, C., Vallejo, W., Campos, K., Solano, W., Andrade, J., Muñoz-Acevedo, A., Schott, E., Zarate, X. (2018). Improvement of the photocatalytic activity of TiO_2 using Colombian Caribbean species (Syzygium cumini) as natural sensitizers: Experimental and theoretical studies. *Dyes and Pigments*, 150, 370–376. DOI: 10.1016/j.dyepig.2017.12.027

[2] Rajagopal, S., Paramasivam, B., Muniyasamy, K. (2020). Photocatalytic removal of cationic and anionic dyes in the textile wastewater by H_2O_2 assisted TiO_2 and microcellulose composites. *Separation and Purification Technology*, 252, 117444. DOI: 10.1016/j.seppur.2020.117444

[3] Wu, M., Shi, L., Lim, T.T., Veksha, A., Yu, F., Fan, H., Mi, J. (2018). Ordered mesoporous Zn-based supported sorbent synthesized by a new method for high-efficiency desulfurization of hot coal gas. *Chemical Engineering Journal*, 353, 273–287. DOI: 10.1016/j.cej.2018.07.134

[4] Lihitkar, P.B., Violet, S., Shirolkar, M., Singh, J., Srivastava, O.N., Naik, R.H., Kulkarni, S.K. (2012). Confinement of zinc oxide nanoparticles in ordered mesoporous silica MCM-41. *Materials Chemistry and Physics*, 133(2–3), 850–856. DOI: 10.1016/j.matchemphys.2012.01.106

[5] Ali, A., Shoeb, M., Li, Y., Li, B., Khan, M.A. (2020). Enhanced photocatalytic degradation of antibiotic drug and dye pollutants by graphene-ordered mesoporous silica (SBA 15)/TiO_2 nanocomposite under visible-light irradiation. *Journal of Molecular Liquids*, 324, 114696. DOI: 10.1016/j.molliq.2020.114696

[6] Brossault, D.F.F., McCoy, T.M., Routh, A.F. (2021). Self-assembly of TiO_2/Fe_3O_4/SiO_2 microbeads: A green approach to produce magnetic photocatalysts. *Journal of Colloid and Interface Science*, 584, 779–788. DOI: 10.1016/j.jcis.2020.10.001

[7] Dhokpande, S.R., Kaware, J.P., Kulkarni, S.J. (2013). Research For Removal Of Nickel From Waste Water - A Review. *International Journal of Science, Engineering and Technology Research (IJSETR)*, 2 (12), 2162–2166. DOI: 10.3282/ijster,20132166

[8] Wang, J., Shao, X., Zhang, Q., Ma, J., Ge, H. (2018). Preparation and photocatalytic application of magnetic Fe_2O_3/SBA-15 nanomaterials. *Journal of Molecular Liquids*, 260, 304–312. DOI: 10.1016/j.molliq.2018.03.109

[9] Ahmed, M.B., Zhou, J.L., Ngo, H.H., Guo, W., Thomaidis, N.S., Xu, J. (2017). Progress in the biological and chemical treatment technologies for emerging contaminant removal from wastewater: A critical review. *Journal of Hazardous Materials*, 323, 274–298. DOI: 10.1016/j.jhazmat.2016.04.045

[10] Miao, J., Liu, B. (2016). Cadmium selenide-sensitized upright-standing mesoporous zinc oxide nanosheets for efficient photoelectrochemical H_2 production. *Journal of Energy Chemistry*, 25(3), 371–374. DOI: 10.1016/j.jechem.2016.02.013

[11] Ulfa, M., Prasetyoko, D., Mahadi, A.H., Bahruji, H. (2020). Size tunable mesoporous carbon microspheres using Pluronic F127 and gelatin as co-template for removal of ibuprofen. *Science of The Total Environment*, 711, 135066. DOI: 10.1016/j.scitotenv.2019.135066

[12] Samadi, M., Zirak, M., Naseri, A., Khorashadizade, E., Moshfegh, A.Z. (2016). Recent progress on doped ZnO nanostructures for visible-light photocatalysis. *Thin Solid Films*, 605, 2–19. DOI: 10.1016/j.tsf.2015.12.064

[13] Ramalingam, R.J., Shukla, A.K., Kombaiah, K., Vijaya, J.J., Tawfeek, A.M. (2017). Synthesis, characterization and optical properties of sulfur and fluorine doped ZnO nanostructures for visible light utilized catalysis. *Optik*, 148, 325–331. DOI: 10.1016/j.ijleo.2017.08.129

[14] Hu, C., Hu, X., Li, R., Xing, Y. (2020). MOF derived ZnO/C nanocomposite with enhanced adsorption capacity and photocatalytic performance under sunlight. *Journal of Hazardous Materials*, 385, 121599. DOI: 10.1016/j.jhazmat.2019.121599

[15] Calzada, L.A., Castellanos, R., García, L.A., Klimova, T.E. (2019). TiO_2, SnO_2 and ZnO catalysts supported on mesoporous SBA-15 versus unsupported nanopowders in photocatalytic degradation of methylene blue. *Microporous and Mesoporous Materials*, 285, 247–258. DOI: 10.1016/j.micromeso.2019.05.015

[16] Babu, K.S., Reddy, A.R., Sujatha, C., Reddy, K.V. (2013). Effects of precursor, temperature, surface area and excitation wavelength on photoluminescence of ZnO/mesoporous silica nanocomposite. *Ceramics International*, 39(3), 3055–3064. DOI: 10.1016/j.ceramint.2012.09.085

[17] Trisunaryanti, W., Sumbogo, S.D., Novianti, S.A., Ayu, D. (2021). ZnO-Activated Carbon Blended as a Catalyst for Oxidative Desulfurization of Dibenzothiophene. *Bulletin of Chemical Reaction Engineering & Catalysis*, 16(4), 881–887. DOI: 10.9767/bcrec.16.4.11797.881-887

[18] Méndez, F.J., Franco-López, O.E., Díaz, G., Gómez-Cortés, A., Bokhimi, X., Klimova, T.E. (2020). On the role of niobium in nanostructured Mo/Nb-MCM-41 and NiMo/Nb-MCM-41 catalysts for hydrodesulfurization of dibenzothiophene. *Fuel*, 280, 118550. DOI: 10.1016/j.fuel.2020.118550

[19] Lolage, M., Parida, P., Chaskar, M., Gupta, A., Rautaray, D. (2020). Green Silica: Industrially scalable & sustainable approach towards achieving improved "nano filler – Elastomer" interaction and reinforcement in tire tread compounds. *Sustainable Materials and Technologies*, 26, e00232. DOI: 10.1016/j.susmat.2020.e00232

[20] Rehman, F., Ahmed, K., Rahim, A., Muhammad, N., Tariq, S., Azhar, U., Jamal, A., Zaib, S., Volpe, P.L.O., Airoldi, C. (2018). Organo-bridged silsesquioxane incorporated mesoporous silica as a carrier for the controlled delivery of ibuprofen and fluorouracil. *Journal of Molecular Liquids*, 258, 319–326. DOI: 10.1016/j.molliq.2018.03.057

[21] Jose, M.G.-G., Maria, V., Pardo, O., Francisco, J.S., Climent, V., Feliu, J.M., Herrero, E. (2021). On the Behavior of CTAB/CTAOH adayer on gold single crysta surface. *Electrochim Acta*, 391, 138947. DOI: 10.1016/j.electacta.2021.138947

[22] Damke, G.M.Z.F., Damke, E., de Souza Bonfim-Mendonça, P., Ratti, B.A., de Freitas Meirelles, L.E., da Silva, V.R.S., Gonçalves, R. S., César, G. B., de Oliveira Silva, S., Caetano, W., Hioka, N., Souza, R.P., Consolaro, M.E.L. (2020). Selective photodynamic effects on cervical cancer cells provided by P123 Pluronic®-based nanoparticles modulating hypericin delivery. *Life Sciences*, 255, 117858. DOI: 10.1016/j.lfs.2020.117858

[23] Petkova-olsson, Y., Oelschlaeger, C., Ullsten, H., Järnström, L. (2018). Journal of Colloid and Interface Science Structural , microrheological and kinetic properties of a ternary silica-Pluronic F127-starch thermosensitive system. *Journal of Colloid and Interface Science*, 514, 459–467. DOI: 10.1016/j.jcis.2017.12.051

[24] Kéri, M., Forgács, A., Papp, V., Bányai, I., Veres, P., Len, A., Dudás, Z., Fábián, I., Kalmár, J. (2020). Gelatin content governs hydration induced structural changes in silica-gelatin hybrid aerogels – Implications in drug delivery. *Acta Biomaterialia*, 105, 131–145. DOI: 10.1016/j.actbio.2020.01.016

[25] Gum, I.G., Bionanocomposites, M., Dziadkowiec, J., Mansa, R., Quintela, A., Rocha, F., Detellier, C. (2017). Applied Clay Science Preparation , characterization and application in controlled release of. *Applied Clay Science*, 135, 52–63. DOI: 10.1016/j.clay.2016.09.003

[26] Ulfa, M., Trisunaryanti, W., Falah, I.I., Kartini, I. (2016). Wormhole-Like Mesoporous Carbons from Gelatine as Multistep Infiltration Effect. *Indonesian Journal of Chemistry*, 16(3), 239–242. DOI: 10.22146/ijc.21137

[27] Ulfa, M., Prasetyoko, D., Bahruji, H., Nugraha, R.E. (2021). Green Synthesis of Hexagonal Hematite (α-Fe_2O_3) Flakes Using Pluronic F127-Gelatin Template for Adsorption and Photodegradation of Ibuprofen. *Materials*, 14(22), 6779. DOI: 10.3390/ma14226779

[28] Sachithanadam, M., Joshi, S.C. (2014). A new phenomenon of compressive strain recovery in gelatin-silica aerogel composites with SDS. *Procedia Engineering*, 75, 51–55. DOI: 10.1016/j.proeng.2013.11.010

[29] An, J., Gou, Y., Yang, C., Hu, F., Wang, C. (2013). Synthesis of a biocompatible gelatin functionalized graphene nanosheets and its application for drug delivery. *Materials Science and Engineering: C*, 33(5), 2827–2837. DOI: 10.1016/j.msec.2013.03.008

[30] Coradin, T., Bah, S., Livage, J. (2004). Gelatine/silicate interactions: From nanoparticles to composite gels. *Colloids and Surfaces B: Biointerfaces*, 35(1), 53–58. DOI: 10.1016/j.colsurfb.2004.02.008

[31] Elzoghby, A.O. (2013). Gelatin-based nanoparticles as drug and gene delivery systems: Reviewing three decades of research. *Journal of Controlled Release*, 172(3), 1075–1091. DOI: 10.1016/j.jconrel.2013.09.019

[32] Fatimah, I., Fadillah, G., Sahroni, I., Kamari, A., Sagadevan, S., Doong, R.A. (2021). Nanoflower-like composites of ZnO/SiO_2 synthesized using bamboo leaves ash as reusable photocatalyst. *Arabian Journal of Chemistry*, 14(3), 102973. DOI: 10.1016/j.arabjc.2020.102973

[33] Nguyen, Q.N.K., Yen, N.T., Hau, N.D., Tran, H.L. (2020). Synthesis and Characterization of Mesoporous Silica SBA-15 and ZnO/SBA-15 Photocatalytic Materials from the Ash of Brickyards. *Journal of Chemistry*, 2020, 8456194. DOI: 10.1155/2020/8456194

[34] Zhiqiang, S., Zhang, J., Han, Y., Hun, B., Yi, L., Zhang, H., Zhao, Y. (2022). Mechanisme of frezing silica gel reaction induced by compaction pressure of ice crystals. *Materials Letters*, 292, 129654. DOI: 10.1016/j.matlet.2021.129654

[35] Abdul-Kadhim, W., Deraman, M.A., Abdullah, S.B., Tajuddin, S.N., Yusoff, M.M., Taufiq-Yap, Y.H., Rahim, M.H.A. (2017). Efficient and reusable iron-zinc oxide catalyst for oxidative desulfurization of model fuel. *Journal of Environmental Chemical Engineering*, 5(2), 1645–1656. DOI: 10.1016/j.jece.2017.03.001

[36] Ulfa, M., Prasetyoko, D., Bahruji, H., Trisunaryanti, W., Nimah, Y.L. (2020). Synthesis of ordered nanoarrays activated carbon using SBA-15 as hard template for adsorption of ibuprofen. *Malaysian Journal of Analytical Sciences*, 24(6), 992–1001. DOI: 10.1015/mjas.2020.127810.

[37] Wei, X., Wang, X., Pu, Y., Liu, A., Chen, C., Zou, W., Zheng, Y., Huang, J., Zhang, Y., Yang, Y., Naushad, M., Gao, B., Dong, L. (2021). Facile ball-milling synthesis of CeO_2/g-C_3N_4 Z-scheme heterojunction for synergistic adsorption and photodegradation of methylene blue: Characteristics, kinetics, models, and mechanisms. *Chemical Engineering Journal*, 420, 127719. DOI: 10.1016/j.cej.2020.127719

[38] Pouretedal, H.R., Kadkhodaie, A. (2010). Synthetic CeO_2 Nanoparticle Catalysis of Methylene Blue Photodegradation : Kinetics and Mechanism. *Chinese Journal of Catalysis*, 31 (11–12), 1328–1334. DOI: 10.1016/S1872-2067(10)60121-0

[39] Wei, J.Q., Chen, X.J., Wang, P.F., Han, Y.B., Xu, J.C., Hong, B., Jin, H.X., Jin, D.F., Peng, X.L., Li, J., Yang, Y.T., Ge, H.L., Wang, X.Q. (2018). High surface area TiO_2/SBA-15 nanocomposites: Synthesis, microstructure and adsorption-enhanced photocatalysis. *Chemical Physics*, 510, 47–53. DOI: 10.1016/j.chemphys.2018.05.012

[40] Ingale, P., Knemeyer, K., Piernavieja Hermida, M., Naumann d'Alnoncourt, R., Thomas, A., Rosowski, F. (2020). Atomic Layer Deposition of ZnO on Mesoporous Silica: Insights into Growth Behavior of ZnO via In-Situ Thermogravimetric Analysis. *Nanomaterials*, 10, 981. DOI: 10.3390/nano10050981